PERGAMON

International Journal of Multiphase Flow 27 (2001) 1861–1879

International Journal of Multiphase Flow

www.elsevier.com/locate/ijmulflow

ADE approach to predicting dispersion of heavy particles in wall-bounded turbulence

Stefano Cerbelli, Andrea Giusti, Alfredo Soldati *

Dipartimento di Scienze e Tecnologie Chimiche, Centro Interdipartimentale di Fluidodinamica e Idraulica, Università di Udine, I-33100 Udine, Italy

Received 27 November 2000; received in revised form 7 May 2001

Abstract

Experiments and numerical computations have highlighted that heavy particles entrained in wall-bounded (e.g. nonhomogeneous) turbulent flows tend to attain a nonuniform distribution in the normal-to-the-wall direction, with higher concentrations near the wall. Recently, a Eulerian model for predicting particle deposition rates that explains the experimental observations on the basis of turbophoretic force was presented. This force causes particles to gain a net drift velocity down the gradients of turbulence intensities. In this paper, we investigate the feasibility of the Eulerian approach for modeling the phenomenology of turbulent dispersion in pipe flow with reflecting walls. Model predictions are compared with original results obtained through direct numerical simulations (DNS) and Lagrangian particle tracking in a turbulent pipe flow ($Re = 4900$). We show that the direct implementation of the model proposed recently tends to overpredict concentration peaks at the pipe wall, a trend that had already been observed in the context of deposition theory (perfectly absorbing wall). We propose a modified model for computing turbophoretic drift velocity by providing an estimate for a term that was considered negligible in the original formulation of the particle momentum balance equation. A better agreement (order of magnitude) between DNS results and model predictions is found.

1. Introduction and background

The physics of inertial particle dispersion by the action of a turbulent carrier flow is a phenomenon of fundamental importance in a variety of contexts, ranging from transport of solid and liquid pollutants in the atmosphere to industrially oriented applications such as the design and optimization of multiphase reactors, deposition of solid particulate in combustion devices, and the

* Corresponding author. Tel.: +39-0-432-558864; fax: +39-0-432-558803.
E-mail address: alfredo.s@uniud.it (A. Soldati).

0301-9322/01/$ - see front matter
PII: S0301-9322(01)00036-2

precipitation of polymeric aggregates in oil pipelines. In cases where the loading fraction of the dispersed phase is small, the theoretical and computational framing of the problem is simplified by the so-called one-way coupling assumption based on the hypothesis that the dispersed phase does not alter the fluid dynamics of the continuous phase. In this case, individual particle trajectories can be determined *a posteriori*, once the flow field has been computed. This Lagrangian approach to turbulent dispersion has been the object of intense computational and theoretical investigation, starting in the early 1950s (see for example Yeung and Pope, 1989 and cited literature).

More recently, detailed descriptions of the fluctuating field of the carrier fluid obtained through direct numerical simulation (DNS) techniques have made it possible to compute detailed statistics of swarms of particles without recourse to turbulence modeling (see, for example, Uijttewaal and Oliemans, 1996; Soldati et al., 1993; and cited literature).

Although these computational studies have undoubtedly contributed to clarifying the mechanisms of convective transport in diluted multiphase turbulent flows, there is still a debate about how to use the results obtained to derive a Eulerian description of particle motion, which is the basis for designing optimal industrial processes.

On the other hand, the Eulerian advection–diffusion–equation (ADE) models that have been proposed in the literature are not completely predictive in that they depend upon phenomenological constants that need to be estimated by experiment or costly simulation (Soldati et al., 1997; Soldati, 2000).

While theories on how to link effective diffusivities to Lagrangian dispersion features of inertial particles are available for homogeneous turbulence (Reeks, 1977), the situation is more complicated in the presence of solid boundaries, which cause the intensity of turbulent velocity fluctuations to be strongly dependent on the normal-to-the-wall coordinate (Caporaloni et al., 1975; Reeks, 1983). This feature translates into an ADE whose transport parameters vary spatially, and are therefore much more difficult to estimate.

A step forward towards bridging the Eulerian and Lagrangian approaches has been recently made by Young and Leeming (1997) – hereon referred to as Y&L – who proposed a fully predictive model for particle dispersion in turbulent pipe flows in the context of deposition theory. The model is based upon Reynolds averages of particle mass and momentum balance equations, where particles are regarded as a continuous phase. Although mainly aimed at predicting deposition rates as a function of particle size, the formal apparatus introduced by the Authors explains many of the transport features that had been observed in both experiments and direct Lagrangian simulations (Liu and Agarwal, 1974; Lee et al., 1989; Young and Hanratty, 1991; Brooke et al., 1994).

In the phenomenon of particle dispersion in turbulent bounded flows, possibly, the most striking observation is that heavy particles tend to be propelled away from the core and accumulate at the pipe wall. This behavior has been recognized to be of utmost importance in determining the particle deposition rate (Brooke et al., 1992, 1994).

In this work, we are interested in determining whether the aforementioned approach is able to capture the physics of particle dispersion independently of the hypotheses that are specific to the deposition model assumed by Y&L, where perfectly absorbing walls were considered. In particular, we assume that particles are elastically reflected away from the pipe wall. It should be noted that perfect elastic reflection, i.e. where no dissipation occurs during the collision, is at the other extreme with respect to the perfectly absorbing wall model, in which particle kinetic energy is

completely lost during the collision. Real world cases are apt to fall somewhere between these limiting situations.

From the Eulerian modeling standpoint, elastic reflection translates into a zero net flux of particles at the wall (i.e. particles cannot cross the pipe wall), which acts as a boundary condition in identifying the solution of the particles ADE.

2. DNS and Lagrangian particle tracking

2.1. DNS of the carrier fluid flow

In this work, we exploited a DNS database for computing concentration profiles of inertial particles as they are transported by the turbulent carrier flow (hereon referred to as gas). The Lagrangian particle tracking (see Section 2.2) is based upon the detailed knowledge of fluctuating gas flow.

We simulated a turbulent pipe flow,with $Re = \overline{U}D/\nu_g = 4900$, where $\overline{U}$ is the average velocity, D is the pipe diameter, and ν_g is the fluid kinematic viscosity. The DNS code is based on a finite difference scheme and was developed by Orlandi and Fatica (1997). (For a comprehensive description of the numerical scheme as well as for the details of the code implementation, we refer the reader to the book by Orlandi, 2000.) The code solves for Navier–Stokes equations in a cylindrical domain (length L, radius R, coordinates θ, r, z) in the transformed variables $q_{f,\theta} = rv_\theta, q_{f,r} = rv_r$, and $q_{f,z} = v_z$ (the subscript f stands for "fluid"). Variables are made dimensionless by using outer units (identified by the superscript "-"), i.e. by taking the pipe radius and the ratio $t^* = R/\overline{U}$ as reference length and time units. Periodic boundary conditions at the inlet and outlet sections are imposed while the average pressure drop along the pipe length is continuously updated to maintain the mass flowrate constant. No-slip and impermeability conditions are imposed at the pipe wall.

The aspect ratio of the pipe was set to the value $L/R = 10$. This value ensures that correlations along the axial direction decay practically to zero within half of the domain length. Spatial discretization was generated by introducing $N_\theta \times N_r \times N_z = 65 \times 65 \times 65$ subdivision points in the intervals $[0, 2\pi], [0, R], [0 : L]$ spanned by the independent variables θ, r and z. Points were equally spaced in the θ and z directions, while a nonuniform discretization was used for the radial coordinate, to obtain a finer grid next to the wall (Orlandi and Fatica, 1997). The initial condition was a (perturbed) Poiseulle flow. Starting from this flow field, the solution was advanced through a Runge–Kutta scheme with a time step $\Delta t^- = 0.01$. This value, imposed by numerical stability requirements (i.e. to maintain the Courant number below unity), is approximately equal to $10^{-2}\tau_K$, where τ_K is the Kolmogorov time-scale of fluctuations (Monin and Yaglom, 1975).

The simulation was run until the statistics of both average axial velocity and RMS profiles of azimuthal, radial and axial velocity fluctuations were found to be in agreement with those reported in the literature (Eggels et al., 1994). This resulted in order 10^5 time-steps, corresponding to $t^- = 1000$.

The instantaneous flow field at the final time of the simulation was saved and used as a restart file for particle tracking simulations, which were run for 2×10^3 time-steps.

2.2. Lagrangian particle tracking

Particle tracking simulations aimed to reproduce the physical situation of solid fly ashes dragged by a turbulent ($Re = 4900$) flow of air within a 5 cm diameter vertical pipe. Particle and gas densities were set to $\rho_p = 1000$ and $\rho_g = 1.3$ Kg/m^3, respectively, while a value $\nu_g = 1.57 \times 10^{-5}$ m^2/s was assumed for the kinematic viscosity of the gas. Three values for particle diameter were considered, namely $D_p = 40; 70; 120\mu$, which correspond to particle relaxation time $\tau_p = 4.5 \times 10^{-3}; 1.3 \times 10^{-2}; 3.9 \times 10^{-3}; s$, where $\tau_p = \rho_p D_p^2 / 18 \rho_g \nu_g$.

The particle equations of motion were made dimensionless by using "+" (wall) units, e.g. by taking $\delta_* = \nu_g / u_*$ and $t^* = \nu_g / u_*^2$ as reference length and time units. In these relationships, u_* is the friction velocity defined as $u_* = \sqrt{\tau_w / \rho_g}$, where τ_w is the wall shear stress.

Owing to the geometry of the system, the particle equations of motion were written in transformed variables. The independent variables were chosen as $Q_\theta = r\theta$; r; z, while the dependent variables were defined as $q_\theta = r v_\theta$, $q_r = r v_r$, and $q_z = v_z$. With this choice, the particle momentum balance equation writes:

$$
\begin{aligned}
&\frac{\mathrm{d}Q_\theta^+}{\mathrm{d}t^+} = \frac{q_r^+ Q_\theta^+}{r^{+2}} + \frac{q_\theta^+}{r^+}, \\
&\frac{\mathrm{d}r^+}{\mathrm{d}t^+} = \frac{q_r^+}{r^+}, \\
&\frac{\mathrm{d}z^+}{\mathrm{d}t^+} = q_z^+, \\
&\frac{\mathrm{d}q_\theta^+}{\mathrm{d}t^+} = \frac{C_\mathrm{d}^+}{\tau_p^+}\left(q_{\mathrm{f}_\theta}^+ - q_\theta^+\right) + \left(1 - \frac{\rho_\mathrm{f}}{\rho_p}\right) g_\theta^+ r^+, \\
&\frac{\mathrm{d}q_r^+}{\mathrm{d}t^+} = \frac{C_\mathrm{d}^+}{\tau_p^+}\left(q_{\mathrm{f}_r}^+ - q_r^+\right) + \left(1 - \frac{\rho_\mathrm{f}}{\rho_p}\right) g_r^+ r^+ + \frac{q_r^{+2} + q_\theta^{+2}}{r^{+2}}, \\
&\frac{\mathrm{d}q_z^+}{\mathrm{d}t^+} = \frac{C_\mathrm{d}^+}{\tau_p^+}\left(q_{\mathrm{f}_z}^+ - q_z^+\right) + \left(1 - \frac{\rho_\mathrm{f}}{\rho_p}\right) g_z^+,
\end{aligned}
\tag{1}
$$

where $C_\mathrm{d}^+ = C_\mathrm{d} / C_\mathrm{S}$ is the ratio between the effective drag coefficient $C_\mathrm{d} = 24/Re_\mathrm{p} + 0.44$ and the Stokesian drag coefficient $C_\mathrm{S} = 24/Re_\mathrm{p}$, and the superscript "+" indicates that all variables are made dimensionless with respect to wall units (inner units).

As the focus of the present work is to understand the physics of turbulent dispersion in the most simplified setting, both Saffman and Basset forces have been neglected in writing Eq. (1). Accordingly, only viscous drag has been considered in the Eulerian radial momentum balance (Section 3.2) to derive the particle drift velocity. This is one advantage offered by DNS versus experiments, namely the effect of each force term can be singled out and investigated separately.

The choice of working with the transformed variables q_θ, q_r and q_z allows for a twofold simplification: (i) it enables to bypass the problem that the value of v_θ, v_r at the axis is undetermined because of the numerical scheme used to solve the DNS simulation, and (ii) it reduces the stiffness of the system at the pipe axis ($r = 0$) with respect to the canonical cylindrical coordinates. The

nodal values of q_θ, q_r and q_z provided by the DNS code were interpolated by using a trilinear interpolation scheme in cylindrical coordinates.

Eq. (1) was solved by using a fifth-order adaptive size Runge–Kutta scheme, assuming a time piecewise constant velocity field of the gas phase. In other words, within each time interval of the DNS simulation the gas flow field was considered "frozen". This approximation is justified by the fact that the DNS time-step is much smaller than both the Kolmogorov time-scale of fluctuations based on the volume-averaged viscous dissipation, τ_K, and the particle relaxation time (when expressed in wall units it results in $\Delta t^+_{\mathrm{DNS}} \sim [10^{-2} \div 10^{-1}]\, \tau^+_{\mathrm{p}}$, depending on the value of particle diameter).

From a practical standpoint, Lagrangian particle tracking was performed in parallel with the DNS simulation. We assumed gravity coincident with the axis of the pipe with the mean flow directed upward. The initial condition was generated by randomly distributing order 10^5 particles within the flow domain and assigning to each particle an initial velocity equal to the average velocity of the fluid at the particle initial position. Particles that came closer than half particle diameter to the wall were reflected elastically. Particles that crossed the outlet section were assumed to re-enter the inlet section instantaneously, in line with the periodic boundary condition of the DNS simulation.

Starting from the uniform distribution, radial profiles of particle concentration were computed at fixed intervals of time by subdividing the pipe into order 400 concentric cylindrical shells of approximately equal volume and counting the fraction of particles that fell within each annular volume, i.e. by averaging over the axial and azimuthal coordinates, z and θ, respectively.

Fig. 1 shows the instantaneous particle profiles for different particle diameters at time $t^+ = 578$, corresponding to 10^4 integration time-steps. Concentration profiles are plotted as a function of the

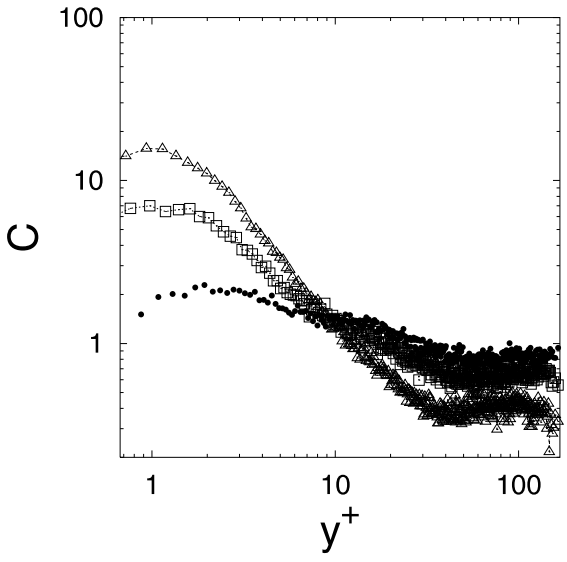

Fig. 1. Instantaneous particle concentration profiles obtained through DNS-Lagrangian tracking at time $t^+ = 580$. The profile are plotted against the wall coordinate y^+ defined by $y^+ = R^+ - r^+$. (●): $D_{\mathrm{p}} = 40\mu$; (□): $D_{\mathrm{p}} = 70\mu$; (△): $D_{\mathrm{p}} = 120\mu$.

dimensionless distance from the wall, $y^+ = R^+ - r^+$ (a logarithmic scale is used to expand the near wall region). As can be observed, in all of the cases considered particles are nonuniformly distributed along the radial coordinate, the trend being more pronounced for larger particles. In particular, the concentration profile appears to reach a maximum very close to the wall ($y^+ \sim 2$) and decrease to lower values towards the pipe axis. This behavior has been observed in both experiments and simulations, almost regardless of the type of particle–wall interaction (more specifically, particle–wall interaction can modify the profile in the near-wall region but does not alter the fact that particles are propelled away from the pipe core region). The physical origin for this behavior has been recognized in the nonuniformity of the gas velocity fluctuations along the pipe radius. Heuristically, an inertial particle located in the core region is subject to higher values of radial fluctuations. Although these fluctuations can occur in both radial directions (i.e. towards or away from the wall), an instantaneous fluctuation towards the pipe wall moves the particle into a region of lower fluctuation intensity, so that the particle is unlikely to be driven back to its original position. This qualitative observation provided the basis for the development of the "free-flight" theory of deposition and has been quantitatively derived by Y&L by considering the Reynolds-averaged Eulerian particle momentum balance (see Section 3.2).

3. ADE approach

3.1. Continuum formulation of particles motion

The ADE approach to particle dispersion consists of regarding the particle phase as a continuum, and writing down the particle mass-conservation equation with respect to a fixed (Eulerian) reference frame. Taking c as the instantaneous value of particle concentration (i.e. the mass of particles per unit volume), and $\mathbf{v}$ the (three-dimensional) Eulerian convective velocity, particle mass balance writes:

$$\frac{\partial c}{\partial t} + \nabla \cdot (\mathbf{v}c) = \nabla \cdot (\mathscr{D}_P \nabla c). \tag{2}$$

The convective motion $\mathbf{v}$ is the consequence of the complex of surface and volume forces that act on individual particles, such as the viscous drag imposed by the surrounding gas, which is in turn a consequence of the different local velocities of gas and particle phase. The diffusive term appearing in the r.h.s. of Eq. (2) accounts for particle motion due to thermal fluctuations. In this context, the total velocity $\mathbf{v}_\mathrm{T}$ of the particle phase is related to the convective velocity, $\mathbf{v}$ by

$$c\mathbf{v}_\mathrm{T} = c\mathbf{v} - \mathscr{D}_\mathrm{p} \nabla c \tag{3}$$

which expresses the total mass flux of particles, $\mathbf{j}_\mathrm{p} = c\,\mathbf{v}_\mathrm{T}$, as the sum of a convective and a diffusive contribution.

Eq. (2) is not very useful in that the instantaneous values of c and $\mathbf{v}$ are in general fluctuating and therefore not accessible to direct experimental measure. Accordingly, a time-averaging (Reynolds averaging) is necessary in order to filter out turbulent fluctuations. This can be accomplished by writing the instantaneous values of c and $\mathbf{v}$ as the sum of an average value and a fluctuating term, i.e.

$$c = C + c', \quad \mathbf{v} = \mathbf{V} + \mathbf{v}', \tag{4}$$

where the average is intended to be taken over by a time-interval long enough to smooth out turbulent fluctuations but short enough to account for variations due to changes in boundary conditions, or to a "macroscopic" transient.

By introducing the notation in Eq. (4) and expanding Eq. (2) in cylindrical coordinates θ, r, z we obtain

$$\frac{\partial C}{\partial t} = -\frac{1}{r}\frac{\partial}{\partial r}(rV_rC) + \frac{1}{r}\frac{\partial}{\partial r}\left[r\mathscr{D}_{\mathrm{p}}\frac{\partial C}{\partial r}\right] - \frac{1}{r}\frac{\partial}{\partial r}\left(r\overline{c'v_r'}\right), \tag{5}$$

where θ and z dependencies have been neglected, consistently with the averaging of DNS-Lagrangian tracking computed concentration profiles over the z and θ coordinates (see previous section). The presence of a net drift velocity $V_r(r)$ is a direct consequence of the embedding of inertial particles in a flow whose turbulent fluctuation intensity is spatially nonhomogeneous. This issue is extensively addressed in the next section. For the time being, we will merely remark that, in order to recover the behavior of passive tracers in the limit of small particles, V_r must converge uniformly to zero as particle diameter decreases to zero.

The term $\mathscr{D}_{\mathrm{p}}\partial C/\partial r$ in Eq. (5) accounts for particle motion due to thermal fluctuations. Clearly, $\mathscr{D}_{\mathrm{p}}$ must decrease to zero for increasing particle diameters. In order to close Eq. (5), the term $\partial(\overline{c'v_r'})/\partial r$ must be expressed in terms of averaged quantities. Following Y&L, we model this term as $\overline{c'v_r'} = \mathscr{D}_{\mathrm{turb}}\partial C/\partial r$ – i.e. the Fickian form, – where the turbulent diffusivity $\mathscr{D}_{\mathrm{turb}}$ is estimated from the gas turbulent viscosity $v_{g,\mathrm{turb}}$ through the turbulent Schmidt number Sc_{turb} (here assumed to be equal to one), i.e. $\mathscr{D}_{\mathrm{turb}} = v_{\mathrm{g,turb}}/Sc_{\mathrm{turb}}$. (the dependency of both $\mathscr{D}_{\mathrm{p}}$ and $v_{\mathrm{g,turb}}$ on particle characteristics and gas fluctuation intensities is reported in Appendix A). With this assumption, Eq. (5) becomes

$$\frac{\partial C}{\partial t} = -\frac{1}{r}\frac{\partial}{\partial r}(rV_rC) + \frac{1}{r}\frac{\partial}{\partial r}\left[r\left(\mathscr{D}_{\mathrm{p}} + \mathscr{D}_{\mathrm{turb}}\right)\frac{\partial C}{\partial r}\right]. \tag{6}$$

From the structure of Eq. (6), it follows that the action of the carrier gas in determining the time evolution of particle concentration emerges both in the turbulent diffusivity, $\mathscr{D}_{\mathrm{turb}}$, and in the radial drift velocity V_r.

Fig. 2 reports the profile of $v_{\mathrm{g,turb}}/v_{\mathrm{g}}$ as a function of normal-to-the-wall coordinate, $y^+ = R^+ - r^+$.

Therefore, for assigned boundary conditions, the solution of Eq. (6) is determined once a suitable expression of V_r as a function of particles parameters and of the radial position is known. Consistently with the DNS-Lagrangian tracking simulation, the boundary conditions are specified by

$$\begin{aligned} &\frac{\partial c}{\partial r}|_{r=0} = 0, \\ &-cV_r + \mathscr{D}_{\mathrm{turb}}\frac{\partial c}{\partial r}\bigg|_{r=R} = 0. \end{aligned} \tag{7}$$

The second of Eq. (7) is the condition of zero net flux at the pipe wall. The first is the same zero flux condition at the pipe axis, where the drift velocity is zero by symmetry.

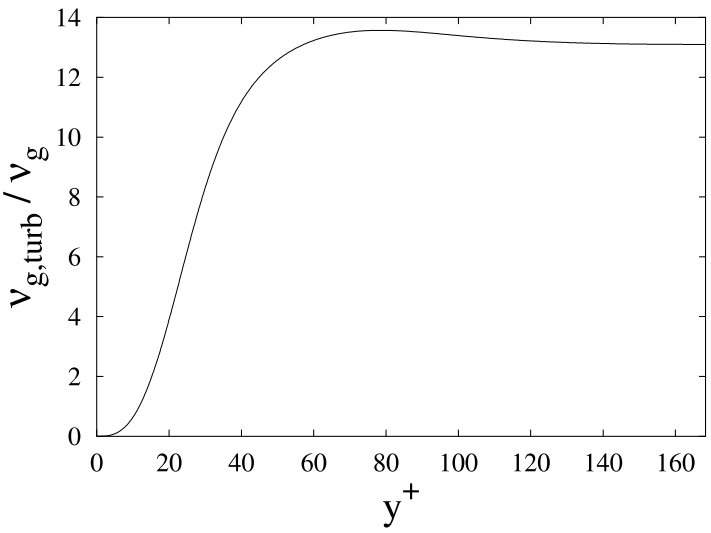

Fig. 2. Profile of the gas turbulent kinematic viscosity, $v_{g,turb}$ (normalized to the molecular kinematic viscosity, v_g) as a function of the normal-to-the-wall coordinate, y^+.

The novelty introduced by Y&L was to derive information about the drift velocity $V_r(r)$ from the Eulerian momentum balance of the dispersed phase, in which the action of the gas is explicitly accounted for. We refer the reader to the original paper for a description of the Reynolds-averaging procedure in the generic three-dimensional framework. In the next Section, only the Reynolds-averaged r-component of momentum balance is reported as the Eulerian approach pursued in this article which aims to model the results of DNS-Lagrangian tracking simulations.

Before analyzing this issue, we will conclude this section by noticing that the Boundary Value Problem expressed by Eqs. (5)–(7) allows for an explicit expression of the steady-state concentration profile

$$C(r) = C_0 \exp\left[\int_0^r \frac{V_r(u)}{\mathscr{D}_p + \mathscr{D}_{turb}(u)}\, du\right], \tag{8}$$

where $C_0 = C(0)$ can be derived by enforcing $\int_0^R 2\pi r C(r)\, dr = M_p$, M_p being the total mass of particles. We notice that the integral in Eq. (8) is always convergent, because of the presence of molecular diffusivity $\mathscr{D}_p$ which makes the denominator bounded away from zero. However, the values of $\mathscr{D}_p$ for typical temperatures and particle diameters are very small whereas the term $\mathscr{D}_{turb}$ is zero at the pipe wall. For this reason, the concentration profile is extremely sensitive to the behavior of the drift velocity $V_r(r)$ in the near-wall region.

From Eq. (8), it is also readily seen that in cases where the drift velocity is uniformly zero, the concentration profile tends towards uniformity, regardless of the fact that $\mathscr{D}_p + \mathscr{D}_{turb}(r)$ depend on r. In other words, *an ADE with variable diffusivity without a convective term cannot explain a nonuniform steady-state profile*.

3.2. Momentum balance and turbophoresis

By using procedures analogous to those outlined in the previous section, and by considering gravity directed along the z-axis (vertical pipe), we obtain the following form for the r component of the momentum balance equation (see, e.g., Y&L for the details of the derivation):

$$V_r \frac{\partial V_r}{\partial r} = -\frac{\Phi_d V_r}{\tau_p} - \frac{\partial}{\partial r}\overline{v_r' v_r'} + \frac{\overline{v_\theta' v_\theta' - v_r' v_r'}}{r} - \overline{v_r' \mathbf{v} \cdot \nabla(\ln\ c)}, \tag{9}$$

where $\mathbf{v}$ and c are the instantaneous values of particle velocity and concentration, respectively (see previous section) and Φ_d is the drag coefficient (here assumed to be equal to one). The contribution of the Saffman lift force has been neglected. In deriving Eq. (9), a pseudo-steady-state assumption has been made, namely that the profile of the drift velocity develops nearly instantaneously for any given profile of particle concentration. This assumption is crucial in order to decouple mass and momentum balance.

The last three terms in the right-hand side of Eq. (9) involve averages of fluctuating quantities, which need to be modeled to close the equation. In Y&L, the last two terms were neglected, as the main contribution to drift velocity was identified in the term involving the gradient $\partial(\overline{v_r' v_r'})/\partial r$ of particle radial fluctuations (*turbophoretic force*).

In particular, the term $\overline{v_r' \mathbf{v} \cdot \nabla(\ln\ c)}$ was dropped by assuming that large values of velocity are always associated with small concentration gradients and vice versa.

However, results of DNS-Lagrangian tracking indicated that, in the presence of reflecting walls, the value of concentration gradients can be very large (Fig. 1). Accordingly, we retain this term and attempt an estimate based on physical arguments. First of all, we assume that $\nabla(\ln\ c) \sim \nabla(\ln\ C)$, since at points where concentration reaches large values, concentration fluctuations are relatively unimportant. Under this assumption, by expanding $\mathbf{v}$ as $\mathbf{v} = \mathbf{V} + \mathbf{v}'$, and neglecting the θ and z components of the velocity we obtain

$$\overline{v_r' \mathbf{v} \cdot \nabla(\ln\ c)} \sim \overline{v_r' v_r'}\ \frac{\partial\ \ln\ C}{\partial r}. \tag{10}$$

A form similar to Eq. (10) was also derived in (Zaichik, 1997) from the probability density function equation describing the transport of particle in the phase space.

By enforcing the pseudo-steady-state hypotesis that was assumed in order to write the stationary r-momentum balance Eq. (9), one can compute the term $\partial(\ln C)/\partial r$ from the steady-state mass balance Eq. (8), thus obtaining

$$\frac{\partial \ln C}{\partial r} = \frac{V_r(r)}{\mathscr{D}_p + \mathscr{D}_{turb}(r)}. \tag{11}$$

The final form of the momentum equation is then given by

$$V_r \frac{\partial V_r}{\partial r} = -\left(\frac{\Phi_d}{\tau_p} + \frac{\overline{v_r' v_r'}}{\mathscr{D}_p + \mathscr{D}_{turb}}\right) V_r - \frac{\partial}{\partial r}\overline{v_r' v_r'}. \tag{12}$$

As suggested in Y&L, the fluctuations of particle radial velocity are related to those of the gas by

$$\overline{v_r' v_r'} = \frac{\tau_g}{\tau_g + \tau_p} \overline{u_r' u_r'}, \tag{13}$$

where $\tau_g = \tau_g(r)$ is a local persistence time of gas turbulent eddies, and $\overline{u_r' u_r'}$ is the square of the RMS radial velocity fluctuations of the gas (the models yielding the profiles of both quantities as a function of y^+ are given in Appendix A). Fig. 3 shows the comparison between $\overline{u_r' u_r'}$ and particles fluctuations $\overline{v_r' v_r'}$ for different particle diameters.

Once particle fluctuations have been modeled, one can solve Eq. (12) for the drift velocity V_r. The initial condition $V_r(r = 0) = 0$ is imposed by symmetry considerations. Eq. (12) is an Abel equation (i.e. nonlinear) and does not yield an analytical solution. In this work, a fourth-order Runge–Kutta scheme was used in order to obtain the numerical solution. Since the Runge–Kutta scheme solves for the normal form of Eq. (12), the equation was solved in the transformed variable z, defined as $z = V_r^2/2$ for $V_r > 0$, and $z = -V_r^2/2$ for $V_r < 0$.

Fig. 4 shows the comparison between the drift velocity profiles computed from Eq. (12) and those obtained from the original formulation of the r-momentum balance of Y&L (e.g. where the term $\overline{v_r' \mathbf{v} \cdot \nabla(\ln c)}$ was neglected) for different particle diameters. For the range of particle diameters considered, the magnitude of the velocity profile monotonically increases with particle diameter (or particle relaxation time τ_p), meaning that larger particles are subject to higher drift velocities. In all cases, the presence of the term of Eqs. (10) and (11) lowers the velocity profiles of corresponding particle diameters. In particular, we can notice that the value of V_r at the pipe wall for the largest particles ($D_p = 120\mu$) is rather different depending on the presence of the term estimated in Eq. (10). As pointed out at the end of the previous section, the behavior of V_r in the near the wall region has a dramatic impact in determining the concentration profiles at long times.

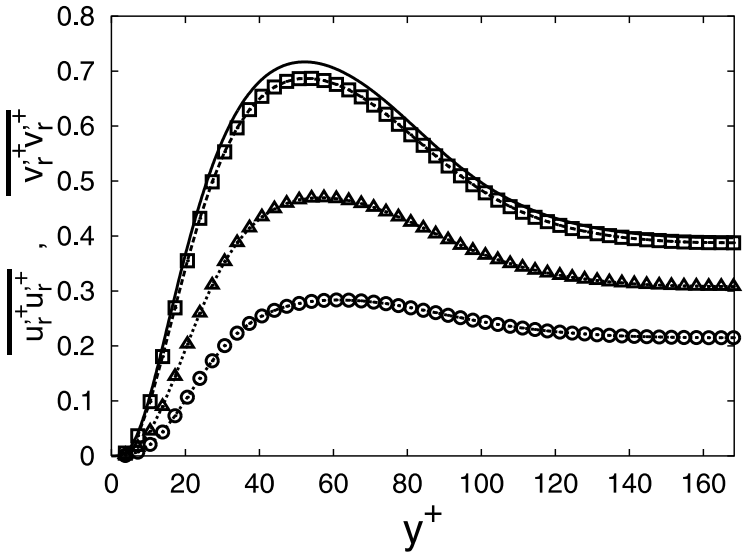

Fig. 3. Intensity of radial fluctuating velocity for the gas ($\overline{u_r'^+ u_r'^+}$) and the particles ($\overline{v_r'^+ v_r'^+}$) as a function of the wall distance y^+. All variables are expressed in wall units. (——): gas; (□): $\tau_p^+ = 0.8$ ($D_p = 20\mu$); (△): $\tau_p^+ = 3.1$ ($D_p = 70\mu$); (○): $\tau_p^+ = 28$ ($D_p = 120\mu$).

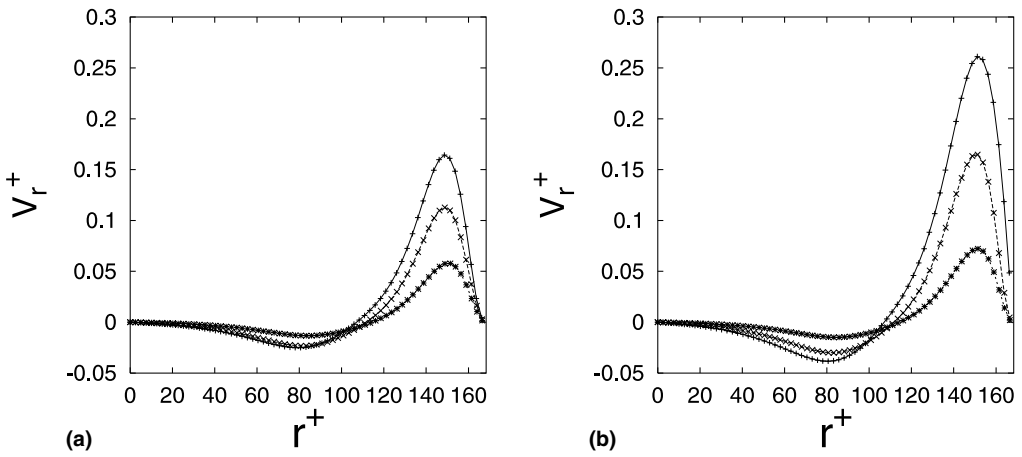

Fig. 4. Profiles of the particle drift velocity for various particle diameters. (a) present model, (b) original momentum balance as proposed by Young and Leeming. (∗)- $D_p = 40\mu$ ($\tau_p^+ = 0.8$); (×)- $D_p = 70\mu$ ($\tau_p^+ = 9.5$); (+)- $D_p = 120\mu$ ($\tau_p^+ = 28$).

4. Results and discussion

Once the drift velocity V_r is known, Eq. (5) constitutes a completely predictive model for the time evolution of particle concentration. Owing to the variable coefficients that are involved, we must resort to numerical integration in order to solve the boundary value problem specified by Eqs. (5)–(7). The steep gradients exhibited by the coefficients impose a finer discretization in the near-wall region. For the numerical solution, we made Eq. (5) dimensionless by normalizing variables with respect to wall ("+") units.

We used a finite-volume semi-implicit scheme (order 400 cells), where the (physical) volumes of the annular sections were chosen to ensure nearuniformity. This leads to consider a subdvision of the $[0, R]$ interval into a nonuniform grid which is finer next to the pipe wall. The finite-volume method adopted does not ensure mass conservation (mass conservation is indeed satisfied by the fully explicit method, which, however, is too demanding in terms of time-step resolution). Specifically, mass was found to increase with time at a rate that depended upon the time-integration step. We fixed a limit of one percent mass production at the final simulation time $t^+ = 1156$, which resulted in a time step of the order $\Delta t^+ = 5 \times 10^{-4}$.

Fig. 5 shows the time evolution of the concentration profile for particle of diameter $D_p = 120\mu$ ($\tau_p^+ = 28$), starting from an initial condition of uniform particle concentration $C(r^+, 0) \equiv 1$, corresponds to a total number of particles $M_p = 1/\pi R^{+2}$. The profiles are taken at intervals of time $\Delta t^+ = 58$, the total simulation time being $T^+ = 1156$ (this value corresponds to 2×10^4 simulation time-steps). A logarithmic scale was chosen to observe the near-the-wall region in detail. The profile develops a maximum, which shifts towards the wall at increasing times until it disappears at the final time considered. Concentration within the core region decreases accordingly, as a net flux of mass occurs towards the pipe wall. The development of a transient maximum can be physically envisioned as a two-stage process characterized by different time-scales. Particles are driven away from the core region by fast convective-diffusion mechanisms, accumulating close to

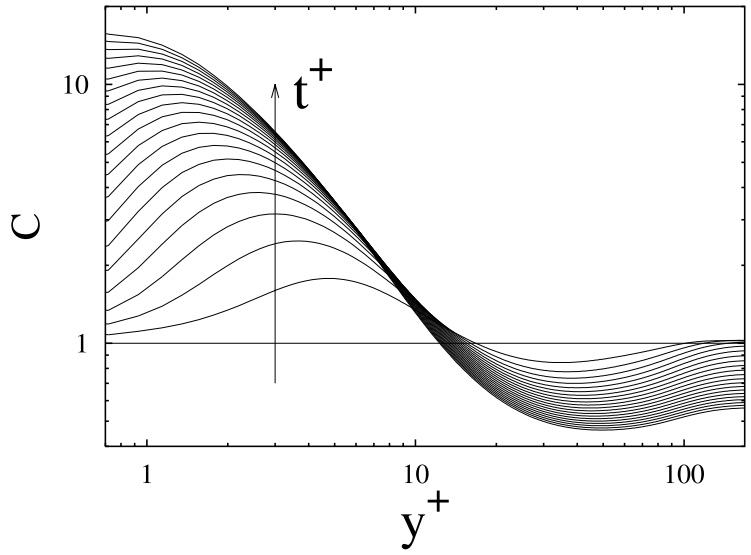

Fig. 5. Transient behavior of concentration profiles for particles of diameter $D_p = 120\mu$ as a function of y^+, obtained by advancing the BVP Eqs. (5)–(7) up to a time $t^+ = 1156$, starting from a flat profile $C(y^+, 0) \equiv 0$ as an initial condition. A maximum in particle concentration profile develops as a consequence of the drift velocity profile profile of Fig. 4. The case shown corresponds to the velocity obtained by solving the modified version of the momentum balance Eq. (12).

the wall, and are then slowly transported towards the pipe wall. Infact, this mechanism has been hypothesized since the early pioneering works on particles deposition (Friedlander and Johnstone, 1954), and the present transient analysis provides support to this conjecture.

Next, we examined the comparison between the ADE model and the DNS simulations. In the remainder, all of the cases shown report the ADE prediction for velocity profiles computed according to the original model by Young and Leeming (1997), and the present model, i.e. where the term $-\overline{v_r' v_r'} \partial \ln C / \partial r$ has been added in the momentum balance equation. We refer to the first case as Y&L, though it is important to emphasize that we are here considering a two-dimensional (z-independent) reduction of the Authors' model for convective velocity, and that we are solving the mass balance ADE Eq. (5) with different boundary conditions at the pipe wall, where we impose zero net flux.

Fig. 6 shows results for the case $D_p = 40\mu$ ($\tau_p^+ = 3.1$). At all times, the ADE solution corresponding to the modified model of drift velocity compares better than the Y&L model with the instantaneous particle concentration profiles obtained through direct Lagrangian tracking. For this value of particle diameter, in both cases the ADE prediction tends to overestimate the concentration peak. At the final time of the simulation, the error predicted by the ADE solution corresponding to the drift velocity profile estimated with the proposed model is sensibly lower than the profile predicted by adopting the Y&L momentum balance equation.

The comparison of model predictions changes dramatically when the particle diameter increases. Fig. 7 shows the results of the same calculations for particle diameter $D_p = 70\mu$. In this case, the drift velocity profiles (Fig. 4) are already sensibly different. This difference presents in the corresponding concentration profiles. The profile in the near-the-wall region is presently overpredicted by the Y&L model and is underpredicted by the proposed model.

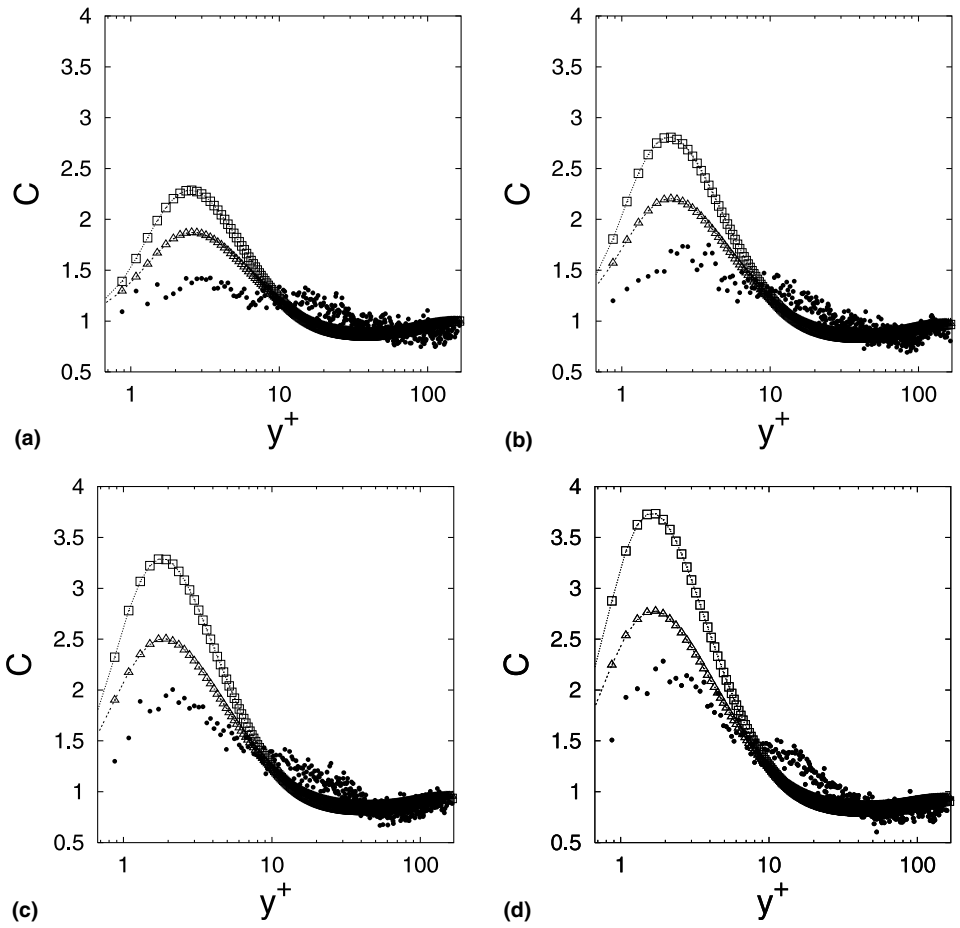

Fig. 6. Comparison at different times of ADE models prediction vs. DNS-Lagrangian tracking simulations for $D_p = 40\mu$. (●): DNS; (△): present model; (□): Y&L. (a) $t^+ = 230$; (b) $t^+ = 350$; (c) $t^+ = 580$; (d) $t^+ = 1050$.

The same trend can be observed for particles of diameter $D_p = 120$. At the final time considered, the prediction error on concentration corresponding to the Y&L velocity profile is much higher (orders of magnitude) than that obtained by considering our estimate for drift velocity (note that the concentration scale is logarithmic). Infact, the velocity profiles (Fig. 4) in the near-the-wall region are considerably different for this value of particle diameter.

A very important question arises as to whether the concentration profiles settle into a stationary behavior, as predicted by the ADE approach (Eq. (8)). Clearly, this point is hard to establish through DNS-Lagrangian tracking techniques since, even should a steady-state exist, the time-scale for obtaining the time-independent behavior could be very long, owing to the low values of drift velocity and turbulent diffusivity in the near-wall region (see Fig. 8).

In order to obtain insights into this point, we ran the DNS-tracking simulation for the $D_p = 120\mu$ particles for a total dimensionless time $t^+ = 2170$, corresponding to order 3.8×10^4 time-steps. We defined a convergence norm, Γ, as $\Gamma = \sum_i |c_i^n - c_i^o| / \sum_i c_i^o$, where c_i^n and c_i^o are the

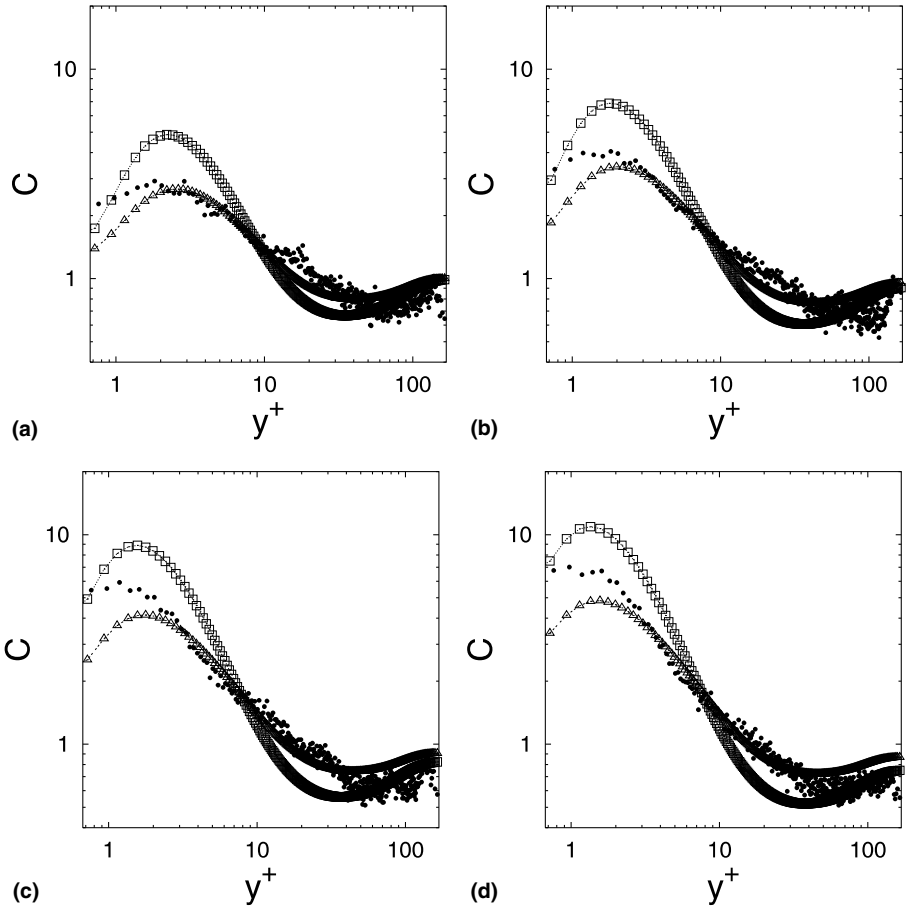

Fig. 7. Comparison at different times of ADE model predictions vs. DNS-Lagrangian tracking simulations for $D_p = 70\mu$. (●): DNS; (△): present model; (□): Y&L. (a) $t^+ = 60$; (b) $t^+ = 260$; (c) $t^+ = 580$; (d) $t^+ = 1050$.

particle concentrations at the spatial locations R_i at different times. Fig. 9 shows the behavior of Γ corresponding to five time instants separated by 2.5×10^3 time steps. As an overall trend, Γ appears to decrease with time, thus indicating that a steady state will be reached eventually (in this condition Γ should be identically zero).

Fig. 10 shows the comparison between the DNS particle concentration profile at the final simulation time $t^+ = 2170$ with the ADE steady-state profiles obtained from Eq. (8). As can be noticed, the Y&L estimate of drift velocity is reflected into a particle concentration profile that for all practical purposes can be considered a Dirac's delta centered at the pipe wall. The present model for computing drift velocity provides instead a quantitative estimate for the DNS data, though it still tends to underpredict concentration in the near-wall region.

Although the ADE model considered in this work must be solved numerically, memory and CPU time requirements are considerably less demanding with respect to the DNS-Lagrangian approach (in all of the cases presented the finite-volume solution of the ADE equation resulted in a CPU time of order 10^{-2} the time required by the DNS simulation). Furthermore, the availability

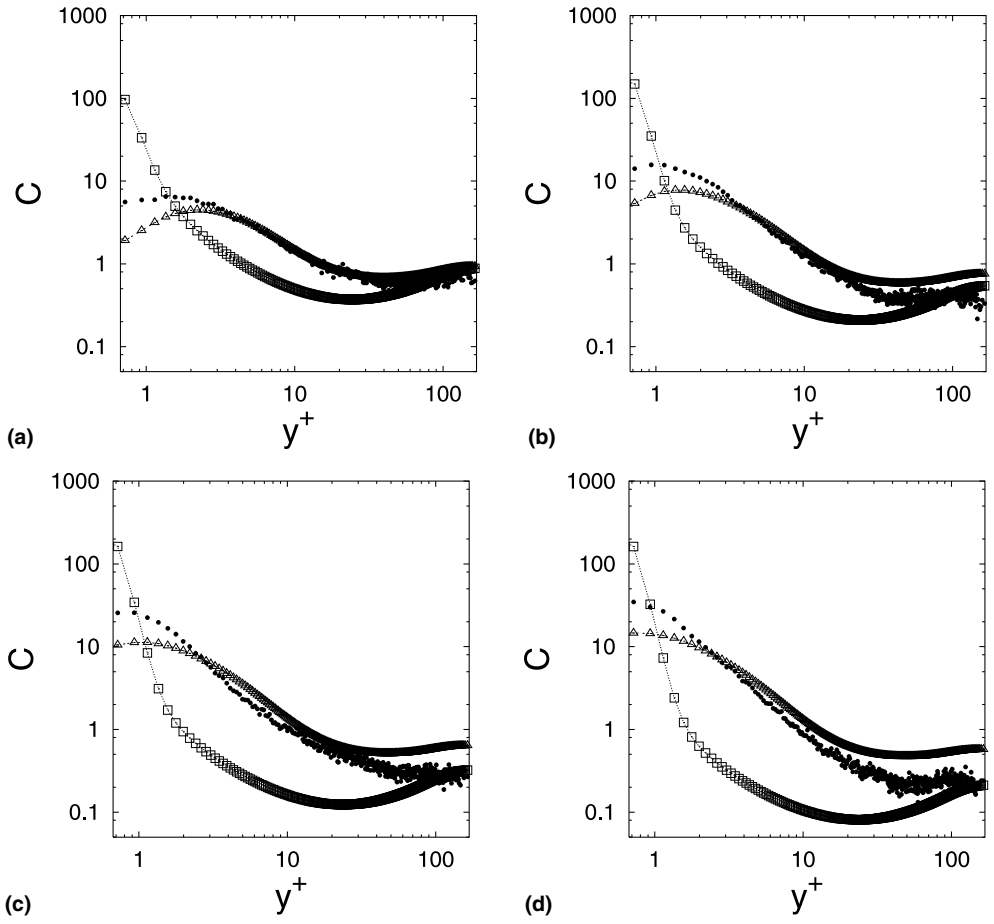

Fig. 8. Comparison at different times of ADE model predictions vs. DNS-Lagrangian tracking simulations for $D_p = 120\mu$. (•): DNS; (△): present model; squares: Y&L. (a) $t^+ = 60$; (b) $t^+ = 260$; (c) $t^+ = 580$; (d) $t^+ = 1050$.

of a fully predictive Eulerian model enables us to gain quantitative insight into the mechanisms of turbulent mixing and to estimate the time-scales at which different mechanisms dominate.

5. Conclusions

In this article, we have proposed a fully predictive Eulerian model for determining the spatiotemporal distribution of inertial particles dispersed by a turbulent carrier flow. The model is based upon the one proposed by Young and Leeming (1997). Our model is different in that we include a term which was neglected in the original formulation. This term involves the product of fluctuating concentration and radial velocity in the radial momentum balance equation (Eq. (10)), and permits to improve by orders of magnitude of the prediction of particle concentration at the wall.

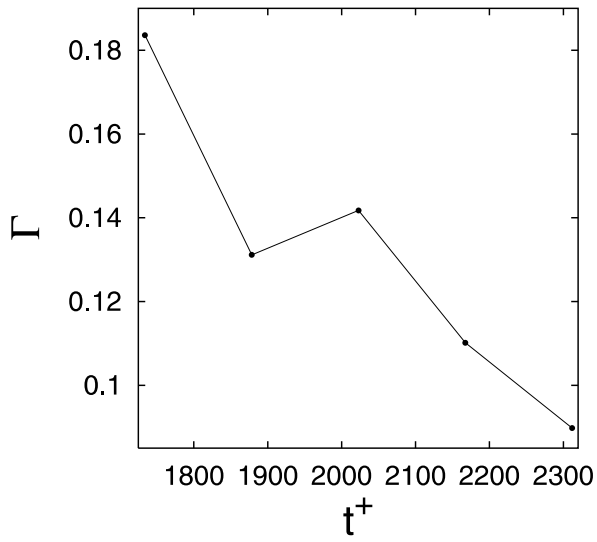

Fig. 9. Convergence towards a steady-state concentration profile (see main text for details).

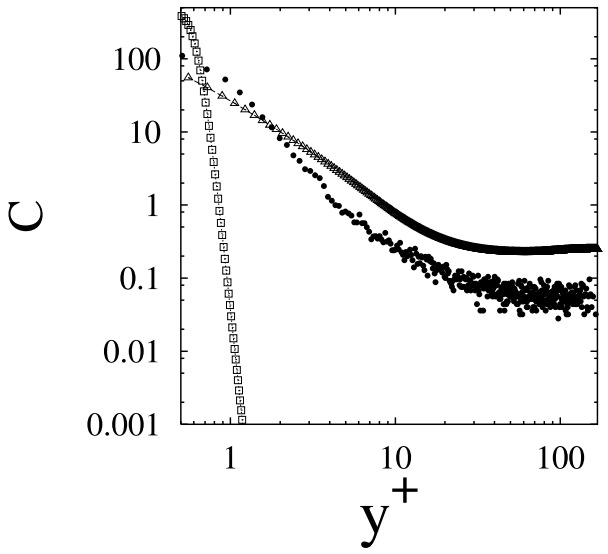

Fig. 10. Comparison of steady-state profiles predicted by the ADE models and the DNS computed profile at the final simulation time $t^+ = 2310$.

The model proposed was validated through original simulations performed through DNS-Lagrangian tracking technique for the case of heavy particles entrained in a turbulent ($Re = 4900$) pipe flow with perfectly reflecting walls. The inclusion of the term neglected by Y&L was found to be crucial in predicting the time-evolution of concentration profiles in the cases examined, especially for the largest ($D_p = 120\mu$) particles. Beyond providing relatively inexpensive quantitative

predictions, the Eulerian approach is also helpful in gaining insights into the mechanisms of turbulent dispersion. The analysis of transient behavior highlighted that radial turbulent transport is characterized by altogether different rates in the core of the pipe and at the wall layer. This shows directly in the time-evolution of particle concentration profiles, which develop a transient maximum near the pipe wall. The maximum moves towards the wall as time increases and eventually disappears, thus yielding a monotonic steady-state profile. This phenomenon, predicted by the Eulerian model, was also indicated by DNS-Lagrangian tracking simulations.

The approach proposed can also be generalized to include wall–particle interactions, which may have a strong impact on practical situations. Indeed, short range forces exchanged between particles and walls can be explicitly accounted for in the momentum balance equation, i.e. by adding a corresponding term in the right-hand side of Eq. (12).

Acknowledgements

Financial support from MURST under Grant 9809326392_005 and Regione FVG under Grant *Fluidodinamica e Analisi delle Dispersioni nella Bassissima Atmosfera del Friuli Venezia Giulia* are gratefully acknowledged. Special thanks to Maria Vittoria Salvetti for the useful discussions.

Appendix A

We report in this appendix the models for both gas and particle fluctuation intensity as proposed in Y&L. Dependencies are given as a function of the normal-to-the-wall coordinate, Y^+. For details, we refer the reader to the references given in Y&L.

A.1. Model of gas eddy viscosity

The gas eddy viscosity is given by a two-layer model that recovers its behavior in the near-wall and and core regions of the pipe, ν_{w+} and ν_{c+}, respectively. The latter are given by

$$\nu_{w+} = \kappa\left[1 - \exp(-y_+^2/\lambda_+^2)\right], \tag{A.1}$$

where $\kappa = 0.4$ and $\lambda_+ = 24$, and

$$\nu_{c+} = \nu_{0+}\left[1.1 - \frac{0.2}{\pi}\arctan\left(\frac{y_+^2}{(R^+ - y_+)^2}\right)\right], \tag{A.2}$$

being $\nu_{0+} = \alpha\overline{U}_{z0+}\delta_+$, with U_{z0+} equal to the centerline velocity, $\alpha = 0.3$ and

$$\delta_+ = \int_0^{R_+} \frac{r_+}{R_+}\left(1 - \frac{\overline{U}_{z+}}{\overline{U}_{z0+}}\right)\mathrm{d}r_+. \tag{A.3}$$

The overall expression of $\nu_{g,turb}/\nu_g$ is given by

$$\nu_{g,turb}/\nu_g = \nu_{c+}\tanh(\nu_{w+}/\nu_{c+}). \tag{A.4}$$

A.2. Model of gas fluctuation intensity

Using analogous symbolism, the gas fluctuation intensities are given by

$$\left(\overline{u'_{y+}u'_{y+}}\right)^{1/2} = u_{c+}\tanh(u_{w+}/u_{c+}), \tag{A.5}$$

where

$$u_{w+} = 0.0373y_+[1-\exp(-y_+/4.67)], \tag{A.6}$$

and

$$u_{c+} = 0.9 - \frac{0.54}{\pi}\arctan\left(y_+^2/(R_+ - y_+)^2\right). \tag{A.7}$$

References

Brooke, J.W., Kontomaris, K., Hanratty, T.J., McLaughlin, J.B., 1992. Turbulent deposition and trapping of aerosols at a wall. Phys. Fluids A 4 (4), 825–833.

Brooke, J.W., Hanratty, T.J., McLaughlin, J.B., 1994. Free-flight mixing and deposition of aerosols. Phys. Fluids 6, 3404–3415.

Caporaloni, M., Tampieri, F., Trombetti, F., Vittori, O., 1975. Transfer of particles in nonisotropic air turbulence. J. Atmos. Sci. (Boston) 32, 565–568.

Eggels, J.G.M, Unger, F., Weiss, M.H., Westerwell, J., Adrian, R.J., Friedrich, R., Nieuwstadt, F.T.M., 1994. Fully developed turbulent pipe flow: a comparison between direct numerical simulation and experiment. J. Fluid Mech. 268, 175–209.

Friedlander, S.K., Johnstone, H.F., 1954. Deposition of suspended particles from turbulent gas streams. Ind. Eng. Chem. Res. 49, 1151–1156.

Lee, M.M., Hanratty, T.J., Adrian, R.J., 1989. An axial viewing technique to study turbulence characteristics of particles. Int. J. Multiphase Flow 15, 787–802.

Liu, B.Y., Agarwal, J.K., 1974. Experimental observation of aerosol deposition in turbulent flow. J. Aerosol Sci. 5, 145–155.

Monin, A.S., Yaglom, A.M., 1975. Statistical Fluid Mechanics, Vol. II. MIT Press, Cambridge, MA.

Orlandi, P., Fatica, M., 1997. Direct simulations of turbulent flow in a pipe rotating about its axis. J. Fluid Mech. 343, 43–72.

Orlandi, P. 2000. Fluid Flow Phenomena. A Numerical Toolkit. Kluwer Academic Publishers, London.

Reeks, M.W., 1977. On the dispersion of small particles suspended in an isotropic turbulent field. J. Fluid Mech. 83, 529–546.

Reeks, M.W., 1983. The transport of discrete particles in inhomogeneous turbulence. J. Aerosol Sci. 14, 729–739.

Soldati, A., 2000. On the effects of electrohydrodynamic flows and turbulence on aerosol transport and collection in wire-plate electrostatic precipitators. J. Aerosol Sci. 31, 293–305.

Soldati, A., Andreussi, P., Banerjee, S., 1993. Direct simulation of turbulent particle transport in electrostatic precipitators. AIChE J. 39, 1910–1919.

Soldati, A., Casal, M., Andreussi, P., Banerjee, S., 1997. Lagrangian simulation of turbulent particle dispersion in electrostatic precipitators. AIChE J. 43, 1403–1413.

Uijttewaal, W.S., Oliemans, R.V.A., 1996. Particle dispersion and deposition in direct numerical and large eddy simulations of vertical pipe flows. Phys. Fluids 8, 2590–2604.

Yeung, P.K., Pope, S.B., 1989. Lagrangian statistics from direct numerical simulations of isotropic turbulence. J. Fluid Mech. 207, 531–586.

Young, B., Hanratty, T.J., 1991. Optical studies on the turbulent motion of solid particles in a pipe flow. J. Fluid Mech. 231, 665–688.

Young, J., Leeming, A., 1997. A theory of particle deposition in turbulent pipe flow. J. Fluid Mech. 340, 129–159.

Zaichik, L.I., 1997. Modelling of the motion of particles in non-uniform turbulent flow using the equation for the probability density function. J. Appl. Mech. 61, 127–133.